Journal of Engineering Mathematics (2024) 148:7
https://doi.org/10.1007/s10665-024-10396-6

# Erosion of surfaces by trapped vortices

**Courteney Hirst**[1] · **N. R. McDonald**[1]

Received: 5 June 2024 / Accepted: 17 August 2024 / Published online: 13 September 2024


**Abstract**
Two two-dimensional free boundary problems describing the erosion of solid surfaces by the flow of inviscid fluid in the presence of trapped vortices are considered. The first problem tackles an initially flat, infinite fluid-solid interface with uniform flow at infinity and a vortex in equilibrium above the surface. The second involves flow around a finite body with a trailing Föppl-type vortex pair. The conformal invariance of the complex potential permits both problems to be formulated as a Polubarinova–Galin (PG) type equation in which the time-dependent eroding surface in the physical $z$-plane is mapped to the fixed boundary of the $\zeta$-disk. The Hamiltonian governing the equilibrium position of the vortex (or vortex pair in the second problem) is also found from the same map. In each problem, the PG equation giving the conformal map is found numerically and the time-dependent evolution of the interface and vortex location is determined. Different models governing the erosion of the interface are investigated in which the normal velocity of the boundary depends on some given function of the fluid flow velocity at the boundary. Typically, in the infinite surface case, erosion leads to the formation of a symmetric valley beneath the vortex which, in turn, moves downward toward the interface. A finite body undergoes erosion which is asymmetric in the flow direction leading to a flattening of the lee surface of the body so displaying some similarity to the experiments and associated viscous theory of Ristroph et al, Moore et al (Proc Natl Acad Sci 109(48):19606–19609, 2012, Phys Fluids 25(11):116602, 2013).

**Keywords** Conformal maps · Erosion · Free boundary · Vortex dynamics

✉ N. R. McDonald
n.r.mcdonald@ucl.ac.uk

Courteney Hirst
courteney.hirst.22@ucl.ac.uk

[1] Department of Mathematics, University College London, Gower St, London, Greater London WC1E 6BT, UK

## 1 Introduction

The erosion of surfaces due to fluid–solid interaction is, in general, a nonlinear free boundary problem [1, 2]. The fluid flow depends on the surface shape which, in turn, undergoes erosion depending on the fluid properties and flow dynamics near the fluid-solid boundary. There is interest in this co-evolution, particularly in geophysical applications [3] where this interaction leads to distinct patterns occurring across multiple length scales such as the smoothness of rocks in streams to the water-driven patterns seen on icebergs. Other examples include ramified stream networks [4], surface scalloping of caves [5–8], yardangs and ventifacts [9], terraces [5, 10], ice-stars [11], and karst pinnacles [12]. In these specific examples, the evolution of the surfaces can result from erosion, abrasion, precipitation, dissolution, or sediment transport and the fluid flow can be that of surface- or ground-water, ocean currents, or wind. Local shedding of vorticity is likely a significant factor in the erosion dynamics e.g., in the scalloping of surfaces, [13] and [14] demonstrate experimentally the close link between vorticity of the flow and the formations of erosion features such as pits and fluting. In engineering applications, computational and numerical studies of the scour that occurs in flow past subsea pipelines often show asymmetry with enhanced scour occurring downstream of the pipeline e.g., References [15, 16]. This, in turn, provides evidence for the enhanced ability of vorticity in the wake to cause local erosion of the sea bed.

One specific class of problems examines the effects of fluid flow in eroding surfaces, where the normal velocity of the evolving interface is proportional to the shear stress exerted by the fluid at the boundary [1, 2], and so necessarily requires that the fluid be viscous. In contrast, the present work assumes the fluid is inviscid and that, instead, the normal velocity of the interface is a function of the tangential velocity of the fluid at the interface. Such an assumption has been used in other work e.g., Reference [17] considers the erosion of solids by fluids in which the normal velocity of the interface depends on a term given by the square of the tangential fluid speed. In this work, models in which the interface erosion depends linearly on the tangential fluid speed, as well as more general forms are considered.

A separate class of problems relevant to the present work is that of finding equilibrium positions of point vortices in two-dimensional potential flow in the presence of bodies such as circular disks, where it is known as the Föppl problem, ellipses, and ‘bumps’ in a plane surface e.g., References [18–22]. In these steady problems, a vortex has equilibrium position depending on its circulation and the background flow speed. This paper shows that, additionally, trapped vortices occur in flow parallel to a plane surface with localized fore-aft symmetric valley-type topography. Specifically, it is shown that the vortex Hamiltonian [19] has closed level curves on the symmetry axis of the valley, which in turn implies the existence of a (stable) vortex equilibrium on this axis. In the finite body problem, the location of the trailing equilibrium vortex pair is also computed numerically from the Hamiltonian.

We consider slowly evolving surfaces. That is, the normal velocity of the surface undergoing erosion is much smaller than the velocity of the fluid flow. This permits a quasi-steady assumption to be made where at any instant of time the surface is considered fixed when determining the flow properties and location of the trapped

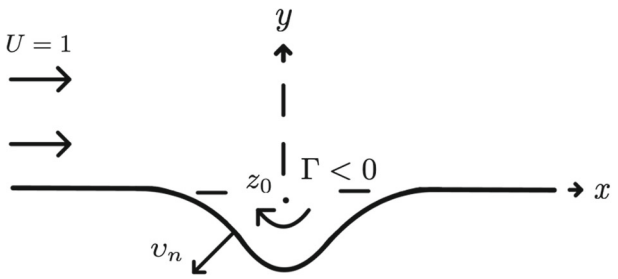


**Fig. 1** A two-dimensional eroding boundary subject to a uniform flow $U = 1$ at infinity and a trapped point vortex with circulation $\Gamma$ at $z = z_0(t)$ in the complex $z$-plane

vortices. A similar assumption is made in [23] in considering potential flow past a body undergoing melting or freezing. Thus, at any time, the vortex maintains equilibrium with respect to the body and external flow. That is, on the slow timescale of the eroding surface, the vortex adjusts its location instantaneously so as to maintain equilibrium.

Away from the point vortices, irrotational flow of an inviscid fluid is assumed. While not explicitly included, viscous effects are implied via the inclusion of trapped vortices since they are often formed by the shedding of vorticity in shear layer separation. The model then allows a description in terms of complex variables with use of methods of conformal mapping and the construction of the vortex Hamiltonian [19].

Section 2 describes the first problem when the eroding fluid-solid body interface is initially an infinitely long, plane surface. It is shown that when the normal velocity of the interface is a function of the local tangential velocity, the evolution of the interface can be described by Polubarinova–Galin (PG) type equation e.g., References [24–27] governing the conformal map from the interior of the unit $\zeta$-disk to the fluid domain in the $z$-plane. Additionally in Sect. 2, the vortex Hamiltonian that governs the instantaneous equilibrium position of the trapped vortex is derived. The PG equation and the location of the equilibrium vortex are solved numerically in Sect. 3 and results are presented for the moving boundary and vortex location for two different erosion laws. Similar techniques are used in Sect. 4 to tackle the second problem of flow past a finite body with a trailing equilibrium vortex pair.

## 2 First problem formulation: plane surface

Consider irrotational flow of an inviscid, incompressible fluid in the $(x, y)$-plane. Let $z = x + \mathrm{i}y$. A point vortex with fixed circulation, $\Gamma$, is initially located at $z = z_0(0)$, $\mathrm{Im}(z_0(0)) > 0$, in a uniform flow with speed $U$ parallel to an infinitely long straight surface aligned with the $\mathrm{Re}(z)$-axis. All quantities are made dimensionless such that the dimensionless uniform velocity at infinity is $U = 1$, and $z_0(0) = \mathrm{i}$. A schematic is shown in Fig. 1, where, after some time, the interface has eroded downwards symmetrically about the imaginary axis and the vortex location $z_0(t)$ has moved downwards from its initial position. The normal velocity of the fluid–solid interface is $v_n$.

The surface is allowed to evolve in accordance with the erosion laws described in Sect. 2.3. Owing to the quasi-steady approximation valid for the slow erosion of the interface, the point vortex maintains a time-varying equilibrium position $z_0(t)$. The erosion law is chosen so as to ensure that the interface evolves symmetrically about the $\mathrm{Im}(z)$-axis. In turn, this implies the equilibrium location of the vortex is on the $\mathrm{Im}(z)$-axis i.e., $\mathrm{Re}(z_0(t)) = 0$. This interaction between the fluid and boundary is a nonlinear free boundary problem and is solved by mapping the problem to the interior of the unit disk in the $\zeta$-plane and determining the necessary conformal map by numerical methods.

A negative (clockwise) vortex circulation $\Gamma$ is required for equilibrium, and it is assumed that the circulation is constant for all time, and it follows for the given initial conditions, $\Gamma = -4\pi$.

On the solid interface, the following boundary conditions apply

$$\mathbf{u} \cdot \hat{\mathbf{n}} = \upsilon_n, \tag{1}$$

and

$$\upsilon_n = \sigma(z), \tag{2}$$

where $\mathbf{u}$ is the fluid velocity, $\hat{\mathbf{n}}$ the normal to the fluid–solid interface which points away from the fluid interior, $\upsilon_n$ is the normal velocity of the slowly eroding surface, and $\sigma(z)$ is a real-valued function giving the imposed normal velocity modeling the erosion—see Sect. 2.3. As in [23], in the fluid flow problem in the slow erosion limit, the boundary condition (1) does not involve the boundary normal velocity $\upsilon_n$ and is given by $\mathbf{u} \cdot \hat{\mathbf{n}} = 0$ so that the boundary is a streamline.

### 2.1 Conformal mappings

Let $z = f(\zeta, t)$ denote the time-dependent map from the interior of the unit $\zeta$-disk to the domain $\Omega$ occupied by the fluid in the $z$-plane. The boundary of the unit $\zeta$-disk, $|\zeta| = 1$, maps to the evolving fluid–solid interface $\partial\Omega$. Furthermore, we introduce an auxiliary plane, the upper half $w$-plane, that is related to both the $\zeta$- and $z$-planes, and is helpful in constructing the vortex Hamiltonian in Sect. 2.2. The relations between all three planes are shown in Fig. 2. The $w$-plane contains a uniform flow, $\overline{U}$, and a point vortex at $w_0$ with circulation, $\Gamma$, and a solid interface coinciding with the $\mathrm{Re}(w)$-axis. The boundaries in the $w$- and $\zeta$-planes remain fixed. The three complex planes are defined by $w = u + \mathrm{i}v$, $\zeta = \xi + \mathrm{i}\eta$, and $z = x + \mathrm{i}y$. The position of the point vortex in each plane is denoted by $w_0$, $\zeta_0$, and $z_0$.

The map

$$\zeta = \frac{\mathrm{i} - w}{\mathrm{i} + w}, \tag{3}$$

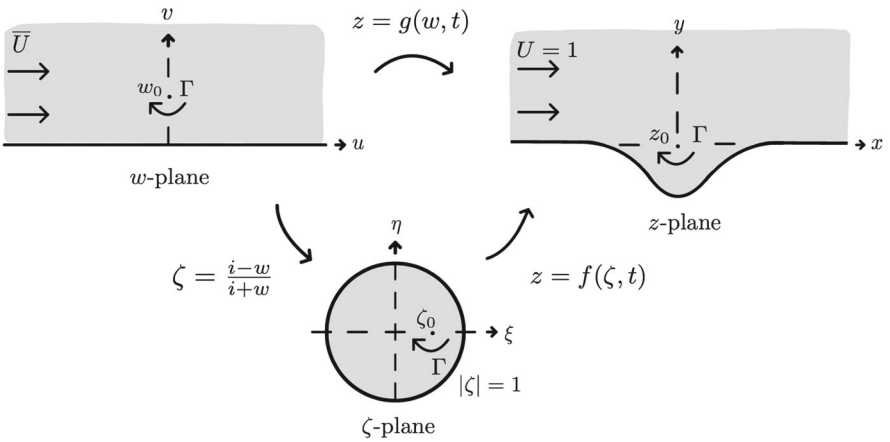


**Fig. 2** Conformal mapping relations between the $z$-, $w$-, and $\zeta$-planes. The shaded region in the physical $z$-plane is $\Omega$ and its boundary $\partial\Omega$ representing the fluid–solid interface is the solid dark line

maps the upper half $w$-plane to the interior of the unit $\zeta$-disk, where $w = \mathrm{i}$ maps to $\zeta = 0$ and these points correspond to the locations of the point vortex in their respective planes at $t = 0$.

In general, the map $z = f(\zeta, t)$ from the $\zeta$- to the $z$-plane can be written as a Laurent series of the form

$$z = \frac{\mathrm{i}A(t)}{\zeta + 1} + \mathrm{i}\sum_{n=0}^{\infty}(a_n(t) + \mathrm{i}b_n(t))\zeta^n, \tag{4}$$

where $A(t)$, $a_n(t)$, $b_n(t)$, for $n = 0, 1, 2, \ldots$, are real, time-dependent, coefficients to be determined. The first term on the RHS of (4) implies that $\zeta = -1$ maps to $z = \infty$ and $w = \infty$. Henceforth, we assume that the eroded interface is symmetric about the $\mathrm{Im}(z)$-axis and so $b_n \equiv 0$, $n = 0, 1, 2, \ldots$.

Since the $w$- and $z$-planes coincide at $t = 0$, it follows $A(0) = 2$, $a_0(0) = -1$ and all other $a_n(0)$ are zero. Furthermore, normalizing by requiring that $\zeta = 0$ maps to $z = \mathrm{i}$ for all time gives the condition

$$A + a_0 = 1. \tag{5}$$

Far from the vortex, we expect the surface to remain flat and aligned with the $\mathrm{Re}(z)$-axis. This requirement can be expressed as $\overline{z} \to z$ on the interface as $z \to \infty$. Taking the conjugate of (4) and using $\overline{\zeta} = \zeta^{-1}$ which holds on the boundary of the unit $\zeta$-disk, we have

$$\overline{z} - z = -\mathrm{i}A - \mathrm{i}\sum_{n=0}^{\infty} a_n(\zeta^{-n} + \zeta^n). \tag{6}$$

Hence, as $z \to \infty$ or, equivalently, $\zeta \to -1$, (6) yields the condition

$$A + 2\sum_{n=0}^{\infty}(-1)^n a_n = 0. \tag{7}$$

In summary, the problem is to find the unknown time-dependent coefficients $A(t)$, $a_n(t)$, subject to the constraints (5), (7), and satisfying the initial conditions $A(0) = 2$, $a_0(0) = -1$, $a_n(0) = 0$ for $n = 1, 2, 3 \ldots$. Sect 2.4 gives the equations satisfied by these coefficients.

### 2.2 Vortex Hamiltonian

The Hamiltonian describing the dynamics of the point vortex in the upper half of the $w$-plane, where the $\mathrm{Re}(w)$-axis is taken to be a wall with zero normal flow, is given by

$$H_w = \Gamma \overline{U} v + \frac{\Gamma^2}{4\pi}\log(v), \tag{8}$$

where $\overline{U}$ is the free stream speed at infinity in the $w$-plane. By comparing the behavior of the free stream speed for large $z$ and large $w$ using the maps (3) and (4), it follows $\overline{U} = AU/2$. To find the Hamiltonian in the $z$-plane, we use the relation connecting the Hamiltonians of conformally mapped domains [19], namely

$$H_z = H_w + \frac{\Gamma^2}{4\pi}\log\left|\frac{\mathrm{d}z}{\mathrm{d}w}\right|, \tag{9}$$

where $\mathrm{d}z/\mathrm{d}w = \partial_w g(w,t)$ is the derivative of the map from the $w$-plane to the $z$-plane, and is calculated using $\mathrm{d}z/\mathrm{d}w = (\mathrm{d}z/\mathrm{d}\zeta)(\mathrm{d}\zeta/\mathrm{d}w)$. Contours of $H_z$ give the vortex trajectories, and the vortex equilibrium position in physical space coincides with extrema of $H_z$, the finding of which is done numerically as described in Sect. 3.

### 2.3 Erosion laws

#### 2.3.1 Model I

Two erosion models are considered both of which are such that the normal velocity of the interface is a function of the local tangential fluid velocity at the interface. In the first, model I, the erosion is assumed to be due to the velocity of the point vortex only, and the free stream contribution is neglected. This prevents the interface from eroding at infinity. Thus,

$$v_n = \beta\left|\frac{\mathrm{d}F_V}{\mathrm{d}z}\right|_{\partial\Omega}, \tag{10}$$

where $\beta > 0$ is a constant, $F_V$ is the complex potential owing to the point vortex only. Note the value of $\beta$ simply affects the timescale for the evolution of the interface and the choice $\beta = 1$ is made throughout the present work. Equation (10) can be written in the $\zeta$-plane as

$$\upsilon_n = \beta \left| \frac{\mathrm{d}F_V}{\mathrm{d}\zeta} \frac{1}{f'} \right|_{|\zeta|=1}, \tag{11}$$

where $f' = \mathrm{d}f/\mathrm{d}\zeta$ and the complex potential inside the unit $\zeta$-disk due to a point vortex at $\zeta = \zeta_0(t)$ is given by

$$F_V(\zeta) = -\frac{\mathrm{i}\Gamma}{2\pi} \log\left( \frac{\zeta - \zeta_0}{\zeta - {\zeta_0}^{-1}} \right), \tag{12}$$

where $\zeta_0 \in \mathbb{R}$ by symmetry. That is, since the vortex remains on the $\mathrm{Im}(z)$-axis, its pre-image $\zeta_0$ is constrained to move on the $\mathrm{Re}(\zeta)$-axis inside the unit disk.

#### 2.3.2 Model II

Model II erosion supposes that the normal velocity of the interface is proportional to the total tangential fluid velocity at the interface, minus the free stream speed $U$. This latter contribution again ensures the interface at infinity does not erode. In mathematical terms,

$$\upsilon_n = \beta \left| \frac{\mathrm{d}F_T}{\mathrm{d}z} - U \right|_{\partial\Omega}, \tag{13}$$

where $F_T$ is the complex potential of the fluid flow field. Equation (13) can be written in the $\zeta$-plane as

$$\upsilon_n = \beta \left| \frac{1}{f'} \left( \frac{\mathrm{d}F_T}{\mathrm{d}\zeta} - f'U \right) \right|_{|\zeta|=1}, \tag{14}$$

where $F_T$ is given by

$$F_T(\zeta) = -\frac{\mathrm{i}\Gamma}{2\pi} \log\left( \frac{\zeta - \zeta_0}{\zeta - {\zeta_0}^{-1}} \right) - \frac{\mathrm{i}AU}{2} \left( \frac{\zeta - 1}{\zeta + 1} \right), \tag{15}$$

where again, $\zeta_0 \in \mathbb{R}$ by symmetry.

### 2.4 The Polubarinova–Galin equations

Equations of the PG type are derived for models I and II, and it is these equations that are ultimately solved to numerically approximate the conformal map $z = f(\zeta, t)$, and with it the surface evolution and vortex location.

The normal velocity of the interface can be written in complex form as

$$\upsilon_n = \hat{\mathbf{n}} \cdot \frac{\mathrm{d}\mathbf{x}}{\mathrm{d}t} = \mathrm{Re}\left[\overline{n_z}\frac{\mathrm{d}z}{\mathrm{d}t}\right], \tag{16}$$

where $\overline{n_z}$ is the conjugate of the complex form of the unit normal vector to the interface $\partial\Omega$. The unit normals in the $z$- and $\zeta$-planes are related by $n_z = f' n_\zeta / \left|f'\right|$ and since $n_\zeta = \zeta$ on the unit $\zeta$-circle, (16) can be expressed as

$$\upsilon_n = \frac{1}{|f'|}\,\mathrm{Re}\left[\overline{f'\zeta}\,\dot{f}\right], \tag{17}$$

where $\dot{f}$ is the time derivative of $z = f(\zeta, t)$. For model I, substituting (12) into (11) and equating to (17) yields

$$\mathrm{Re}\left[\overline{f'\zeta}\,\dot{f}\right] = \frac{\beta\,|\Gamma|}{2\pi}\left|\frac{\zeta_0^2 - 1}{(2\zeta_0\cos\theta - 1 - \zeta_0^2)}\right|, \tag{18}$$

where $\zeta = \exp(\mathrm{i}\theta)$. This is a PG type equation determining the conformal map $f(\zeta, t)$ from the $\zeta$- to $z$-planes which, in turn, gives the evolution of the interface in the $z$-plane due to model I erosion.

Similarly, the PG equation for model II erosion is given by

$$\mathrm{Re}\left[\overline{f'\zeta}\,\dot{f}\right] = \beta\left|\frac{\Gamma}{2\pi}\frac{1-\zeta_0^2}{(2\zeta_0\cos\theta - 1 - \zeta_0^2)} - \frac{AU}{4\cos^2(\theta/2)} + \mathrm{i}\zeta\, f' U\right|. \tag{19}$$

## 3 Numerical solution for the eroding plane surface

### 3.1 Method

The task is to find the unknown conformal map $z = f(\zeta, t)$ (4) that satisfies equations (18) or (19) under the constraints given by (5) and (7), and that the vortex remains in equilibrium for all time. First, the map (4) is approximated by truncating the infinite series at some finite value, $n = N$, giving $N+2$ unknown time-dependent coefficients $A(t), a_0(t), a_1(t), \ldots, a_N(t)$ to be determined. We then use the method from [28] (see also [27]) and apply the PG equation (18) or (19) at $N$ points given by $\zeta_\mathrm{j}$=exp(i$\theta_\mathrm{j}$), j = 1, 2, ..., $N$. Hence, (18) or (19) becomes a system of $N$ coupled ordinary differential equations and together with (5) and (7) can be used to solve for the $N+2$ unknown coefficients in the truncated conformal map. Additionally, at each timestep, the pre-image of the vortex equilibrium location $\zeta_0(t)$ needs to be computed.

To avoid the singularity at $\zeta = -1$ present in (4), and exploiting the symmetry of the interface, the points $\zeta_\mathrm{j}$ are distributed in the interval $0 \le \theta_\mathrm{j} \le \pi - \epsilon$, where $0 < \epsilon \ll 1$ is chosen so that the boundary of the interface in the $z$-plane approximately

extends along the interval [0, 50] of the Re($z$)-axis. This interval is sufficiently large to both capture the features of the erosion and to avoid end-effects.

The system of $N + 2$ equations with $N + 2$ unknowns is solved using MATLAB's *ode15i* routine. At each timestep, the truncated conformal map (4) is used to find the Hamiltonian (9) and its extremal point on the Im($z$)-axis coinciding with the vortex equilibrium $z_0$ and its pre-image $\zeta_0$ is found using MATLAB's *fminsearch*. The numerical procedure for finding the co-evolution of the vortex and interface is summarized in Algorithm 1.

**Algorithm 1** Vortex–plane surface erosion

**Require:** $\beta = 1, U = 1, \Gamma = -4\pi, \epsilon, N, t_{max}$, erosion model I or II
  Set initial map coefficients: $A = 2, a_0 = -1, a_n = 0, n = 1, \ldots, N$
  **while** $t < t_{max}$ **do**
    Ensure $A(t), a_n(t), n = 0, \ldots, N$ satisfy conditions (5) and (7)
    Construct vortex Hamiltonian $H_z$
    Obtain pre-image of vortex equilibrium $\zeta_0(t)$ using *fminsearch*; hence find $z_0(t)$
    Solve PG equation at $\zeta_j$, $j = 1, \ldots, N$ using *ode15i*
    Obtain conformal map coefficients $A(t), a_n(t), n = 0, \ldots, N$
  **end while**

Preliminary testing of the algorithm was done for the special case of model I when the vortex is artificially fixed at $z = \mathrm{i}$ for which an exact solution is available—see Appendix A. With $N = 32$, good agreement was found between the numerically computed eroding interface and that given by (A3) and (A4).

In the full dynamical problem with a moving vortex, truncating (4) at $N = 32$ was found to be effective and accurate based on the convergence testing results: for model I, comparing both interface profiles and vortex equilibrium locations showed negligible difference between $N = 32$ and $N = 64$. However, the numerical scheme for larger values of $N$ (e.g., $N = 128$) failed to converge for $t = \mathcal{O}(1)$. For model II, failure to converge occurs for choices $N \gtrsim 80$. For this reason, convergence testing for model II was done for $N = 16$, 32 and 48, and showed negligible difference between $N = 32$ and $N = 48$.

### 3.2 Results

The following parameter values were fixed: $\beta = 1$, $\Gamma = -4\pi$, and $U = 1$. Figure 3 shows the eroding interface at equal time intervals between $0 \leq t \leq 2$, where (a) and (b) correspond to erosion models I and II, respectively. Model II produces more localized erosion about the axis of symmetry compared to model I, and erodes to a deeper level in the Im($z$) direction over the same time period. In both erosion models, the rate at which the vortex moves downward appears to slow with time as evidenced by the decreasing distance between dots, although this slowing occurs more quickly in model I.

Figure 4a compares the erosion profiles and equilibrium vortex locations when $t = 0.222$ and $t = 2$, where the results of model I are represented in black and model II in blue. For small times, the profiles due to models I and II evolve similarly as

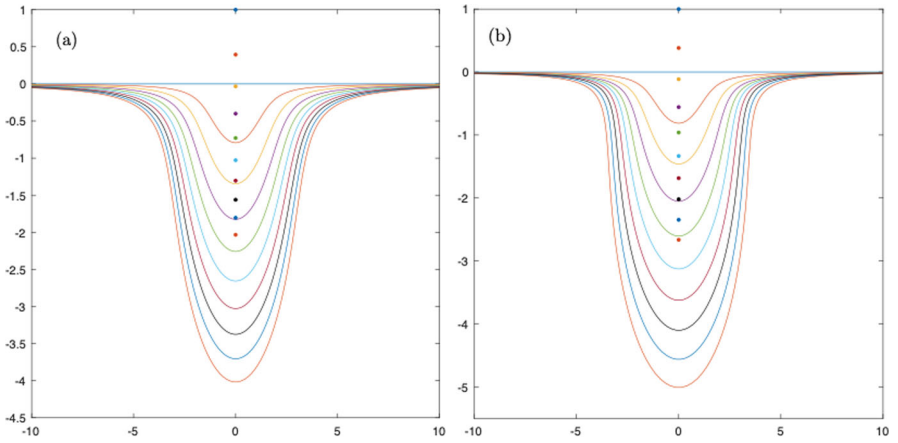


**Fig. 3** **a** and **b** show snapshots at equal time intervals of the eroded interface for erosion models I and II, respectively, for $0 \leq t \leq 2$. Dots show equilibrium vortex locations with the color of each dot corresponding to the same color interface

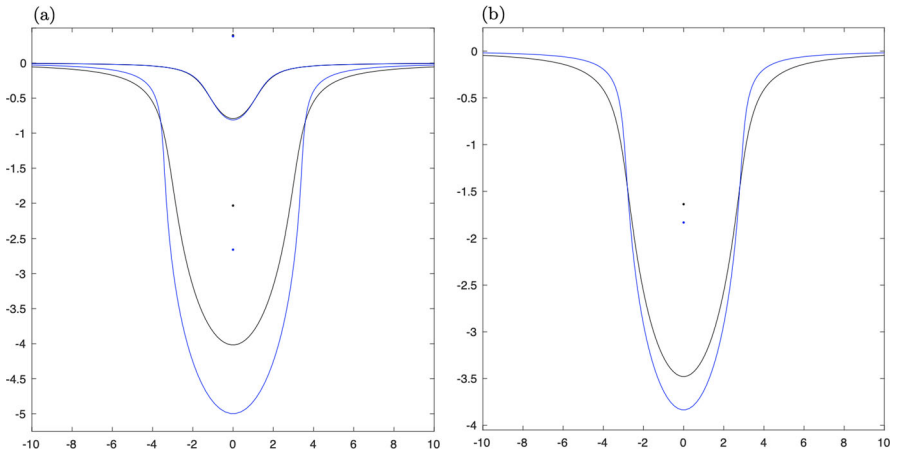


**Fig. 4** Comparison of interfaces and corresponding equilibrium vortex locations for erosion model I (black) and model II (blue): **a** $t = 0.222$ and $t = 2$; **b** interfaces with equal displaced area which occur at $t \approx 1.624$ (model I) and $t \approx 1.431$ (model II)

indicated by them almost coinciding for $t = 0.222$. As time increases, the interface profiles diverge between the two models as shown by their comparison at $t = 2$ in Fig. 4a. An alternative way to compare the interface behavior between the two models is done in Fig. 4b which compares model I and II profiles having the same displaced area of 20 units. The displaced area anomaly (i.e., the area of the eroded region) is computed directly from the conformal map according to the formula (B16) in Appendix B, or directly by numerical integration of the interface profile using MATLAB's *trapz* function.

Figure 5 shows the streamlines and Hamiltonian contours for the topography produced by model I erosion at $t = 2$. The streamlines show the region of recirculation

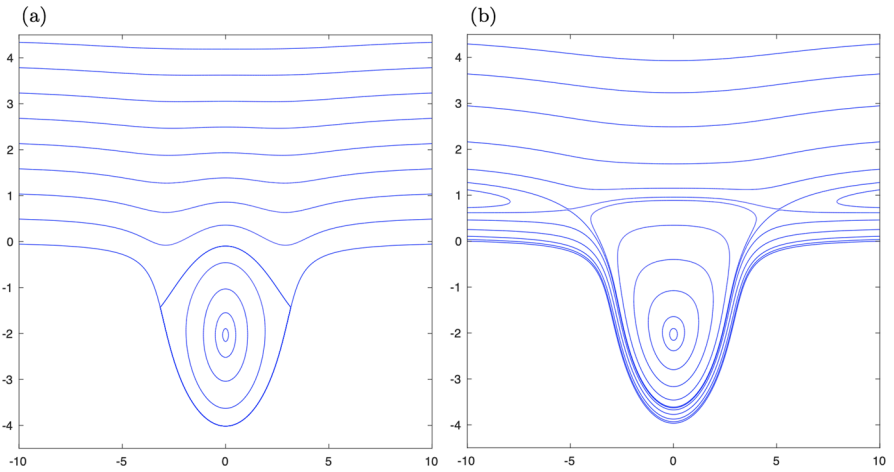


**Fig. 5** Streamlines (**a**) and contours of the Hamiltonian (**b**) for erosion model I at $t = 2$

within the eroded region and the presence of stagnation points on the boundary. The Hamiltonian contours show hyperbolic points for vortex equilibria upstream and downstream of the symmetry axis. These correspond to unstable vortex equilibria. Importantly, the vortex equilibrium on the symmetry axis, as considered here, is stable as indicated by closed contours of the Hamiltonian. The plots shown in Fig. 5 are typical with other choices of parameters, erosion models, and $t$ as all have similar topologies.

As $t$ increases in both erosion models, the interface continues to erode and the vortex moves downward. No steady state in which the erosion is arrested and the vortex becomes stationary was found in any of the numerical experiments. This is expected since with models I and II the tangential velocity is always non-constant on the interface and so $\upsilon_n$ remains non-zero according to (10) or (13). It is worth speculating if there is an erosion law for which a steady state arises. For this to occur it would be necessary for the tangential velocity to become constant on the interface. A possible route to constructing a model with a steady state is to replace the background uniform velocity with a linear shear flow with uniform vorticity. The problem then becomes mathematically similar to finding steady water waves in the presence of submerged vortices. Such solutions have recently been documented and extended in [29]. The possible connection between such water wave solutions with a variant of the present problem is left for future work.

### 3.3 A more general erosion model

A more general form of erosion model I is

$$\upsilon_n = \beta \left| \frac{\mathrm{d}F_V}{\mathrm{d}z} \right|^n_{\partial\Omega}, \tag{20}$$

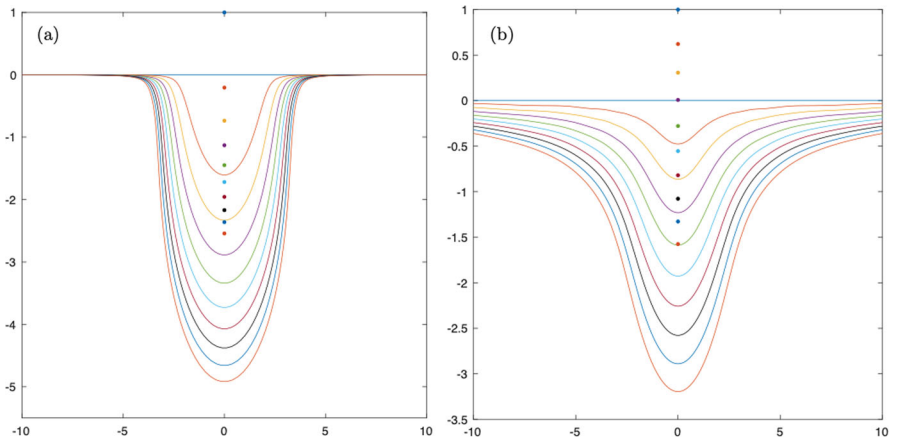


**Fig. 6** Evolution of the interface and corresponding vortex location for the generalized erosion model (20) with **a** $n = 2$ and **b** $n = 1/2$, $0 \le t \le 2$. Dots show equilibrium vortex locations with the color of each dot corresponding to the same color interface

where $n > 0$ is a constant. The PG equation then becomes

$$\mathrm{Re}\left[\overline{f'\zeta}\,\dot{f}\right] = \beta \left|\frac{\Gamma}{2\pi}\right|^n \left|f'\right|^{1-n} \left|\frac{\zeta_0^2 - 1}{2\zeta_0 \cos\theta - \left(\zeta_0^2 + 1\right)}\right|^n, \tag{21}$$

on $\zeta = \exp(\mathrm{i}\theta)$. Numerical results for $n = 2$ and $1/2$ are shown in Fig. 6a and b, respectively. For larger $n$, the erosion becomes more localized being confined to the region $|\mathrm{Re}(z)| \lesssim 4$, while eroding to a deeper extent in the $\mathrm{Im}(z)$-direction. In the small $n$ limit, (20) shows the normal velocity of the interface tends toward a constant. This less localized erosion implies that the numerical method becomes inaccurate over a finite length in the $\mathrm{Re}(z)$-direction. In fact, for $n < 1/2$, convergent results were unable to be found.

## 4 Second problem: an eroding finite body

The second problem considers erosion by two-dimensional flow past a finite body with Föppl-type vortices trapped in the lee of the body. The presence of such vortices is a step toward modeling the effects of viscosity since their presence can be considered a consequence of vorticity shedding in boundary layer separation.

The problem is non-dimensionalized using the initial conformal radius of the body and the flow speed at infinity. To begin, the body is taken to be the unit disk centered at $z = 0$ immersed in a flow speed $U = 1$ parallel to the $\mathrm{Re}(z)$-axis at infinity. Two Föppl, or equilibrium, vortices with fixed equal and opposite circulations $\pm\Gamma$ are located in the lee of the disk and are, necessarily, arranged symmetrically at $z_0(t)$ and $\overline{z_0}(t)$, where $|z_0(0)| > 1$.

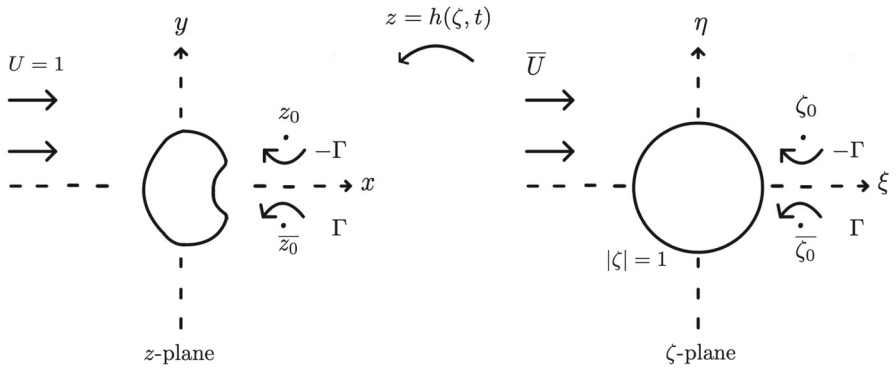


**Fig. 7** Relationship between the finite body ($z$-plane) and the standard flow past the unit disk Föppl ($\zeta$-plane) problem. The conformal map from the exterior of the $\zeta$-disk to the exterior of the body in the $z$-plane is $z = h(\zeta, t)$. Equal but oppositely signed vortices are located in the lee of the body

### 4.1 Conformal mapping and the Hamiltonian

In this problem, we map directly from the exterior of the eroding body in the $z$-plane to the exterior of the unit $\zeta$-disk using

$$z = h(\zeta, t) = C(t)\zeta + \sum_{n=0}^{\infty} c_n(t)\zeta^{-n}, \tag{22}$$

where $C(t)$ and $c_n(t)$, $n = 0, 1, \ldots$, are real time-dependent coefficients, ensuring that the body remains symmetric about the $\mathrm{Re}(z)$-axis as it is eroded. Note that $C(t)$ is the conformal radius of the body. Initially the body is the unit disk centered at the origin so $C(0) = 1$, and $c_n(0) = 0$, $n = 0, 1, \ldots$. The pre-image of the vortex location in the upper part of the $z$-plane is $\zeta_0$ i.e., $z_0(t) = h(\zeta_0, t)$. Initially the vortex pair is in equilibrium, that is, it is a Föppl pair. In this problem, $\zeta_0(t)$ is, in general, complex-valued in contrast to it being real-valued in the infinite interface problem.

In the $\zeta$-plane, the complex velocity potential is

$$F(\zeta) = C(t)\left(\zeta + \zeta^{-1}\right) - \frac{\mathrm{i}\Gamma}{2\pi}\log\left(\frac{\zeta - \zeta_0}{\zeta - \overline{\zeta_0}^{-1}}\right) + \frac{\mathrm{i}\Gamma}{2\pi}\log\left(\frac{\zeta - \overline{\zeta_0}}{\zeta - {\zeta_0}^{-1}}\right), \tag{23}$$

where the coefficient $C(t)$ on the RHS is equivalent to the velocity at infinity $\overline{U}$ in the $\zeta$-plane and ensures that, using (22), $F \to z$ as $z \to \infty$, i.e., $U = 1$ in the $z$-plane as required. Note that the vortex located in the upper half of the $z$-plane must have negative (clockwise) circulation in order to achieve equilibrium. The arrangement for some $t > 0$ is shown in both complex planes in Fig. 7.

The Hamiltonian in the $\zeta$-plane is e.g., Reference [22]

$$H_\zeta = \Gamma C\,\mathrm{Im}(\zeta)\left(1 - \frac{1}{r^2}\right) + \frac{\Gamma^2}{4\pi}\log\frac{\mathrm{Im}(\zeta)(r^2 - 1)}{\sqrt{(r^2 - 1)^2 + 4\,\mathrm{Im}(\zeta)^2}}, \tag{24}$$

where $r = |\zeta|$. In the $z$-plane, symmetry persists about the real axis and so the Hamiltonian is two-dimensional (and not four-dimensional as might be expected for a system of two vortices), $H_z = H_z(x, y)$, and is given by

$$H_z = H_\zeta + \frac{\Gamma^2}{4\pi} \log \left| \frac{\mathrm{d}h}{\mathrm{d}\zeta} \right|. \tag{25}$$

### 4.2 Polubarinova–Galin equation

As in Sect. 2.4, (17) is used to find a PG equation for the conformal map $z = h(\zeta, t)$ for an erosion law specifying $v_n$. By symmetry, the flow has fore and aft stagnation points where body's boundary crosses the $\mathrm{Re}(z)$-axis. This means that for model I and II erosion laws, the body would not erode at these points and this is unrealistic. Instead we consider an erosion law where the normal velocity of the fluid–solid interface is proportional to $|F_{zz}|$:

$$\begin{aligned} v_n &= -\beta |F_{zz}|_{\partial\Omega} \\ &= -\frac{\beta}{|h'|} \left| \frac{\partial F_z}{\partial \zeta} \right|_{\partial\Omega} \\ &= -\frac{\beta}{|h'|^2} \left| F'' - F' \frac{h''}{h'} \right|_{|\zeta|=1}, \end{aligned} \tag{26}$$

where the dashes denote differentiation with respect to $\zeta$ and so

$$F' = C\left(1 - \frac{1}{\zeta^2}\right) - \frac{\mathrm{i}\Gamma}{2\pi}\left[\frac{1}{\zeta - \zeta_0} - \frac{1}{\zeta - \overline{\zeta_0}^{-1}} - \frac{1}{\zeta - \overline{\zeta_0}} + \frac{1}{\zeta - \zeta_0^{-1}}\right], \tag{27}$$

$$F'' = \frac{2C}{\zeta^3} + \frac{\mathrm{i}\Gamma}{2\pi}\left[\frac{1}{(\zeta - \zeta_0)^2} - \frac{1}{\left(\zeta - \overline{\zeta_0}^{-1}\right)^2} - \frac{1}{\left(\zeta - \overline{\zeta_0}\right)^2} + \frac{1}{\left(\zeta - \zeta_0^{-1}\right)^2}\right]. \tag{28}$$

Note that the sign of $v_n$ in (26) is opposite to that of (10) since now the map from the $z$-plane is to the exterior, and not interior, of the unit $\zeta$-disk.

Recall the fluid velocity is $u - \mathrm{i}v = F_z$, thus (26) is a measure of the spatial gradient of the fluid velocity. In this sense, it is dimensionally equivalent to the shear of the velocity field used in other studies of erosion of bodies by fluid flow e.g., References [1, 2], though $F_{zz}$ has no clear interpretation as shear, or other dynamically significant quantity. It is used here owing to its relative simplicity and that (as we shall show) it gives realistic results for the shape of the eroding body. Figure 8 shows the initial form of $|v_n|$ given by (26) (with $\beta = 1$) when the body is a unit disk and so $h' = 1, h'' = 0$ for two different choices of $r_0 = |z_0(0)|$, the distance of the trapped vortices from the body (see Sect. 4.3). Note that the largest magnitude of $v_n$ is at $\theta = 0$ implying that erosion is likely dominant at the rear of the body.

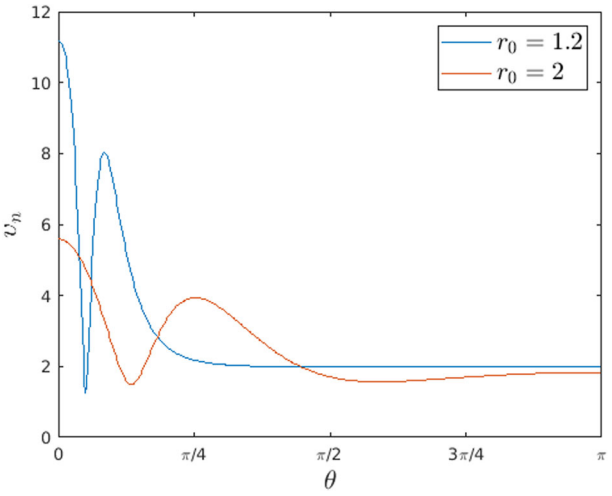


**Fig. 8** The erosional velocity $v_n$ around the circular body at $t = 0$ given by (26) and (28) (ignoring the factor $-\beta$) as a function of $0 \le \theta \le \pi$ for $r_0 = 1.2$ and $r_0 = 2$

Using (17) and (26), the PG equation valid on $\zeta = \exp(\mathrm{i}\theta)$ is

$$\mathrm{Re}\left[\overline{h'\zeta}\dot{h}\right] = -\frac{\beta}{|h'|}\left|F'' - F'\frac{h''}{h'}\right|. \tag{29}$$

### 4.3 Numerical implementation and results

Proceeding similarly to Sect. 3.1, the series (22) is truncated at $n = N$ leaving $N+2$ unknown coefficients $C(t), c_0(t), \ldots, c_N(t)$, to be determined by solving (29) at $N+2$ evenly spaced points $\theta \in [0, \pi]$ on the half $\zeta$-disk. In the results shown $N = 64$, and $\beta = 1$.

Initially, the vortex location $z_0(0) = x_0 + \mathrm{i}y_0$ is chosen to be at distance $r_0 = |z_0(0)| > 1$ from the unit disk. Given the Hamiltonian (24) and the initial data $r_0$ and $C_0 = C(0)$, the constant vortex circulation $\Gamma$ and initial position of the Föppl vortices can be found using formula from [22]:

$$\frac{\Gamma}{C_0} = -2\pi\frac{(r_0^2+1)(r_0^2-1)^2}{r_0^5}, \tag{30}$$

$$2y_0 r_0 = r_0^2 - 1, \tag{31}$$

and $x_0 = \sqrt{r_0^2 - y_0^2} > 0$. In the following, results for the evolution of the body and corresponding equilibrium vortex locations are presented for different choices of $r_0$. When the vortices are initially very close to the surface of the disk, convergent results are difficult to obtain; results are shown here for $r_0 \ge 1.2$.

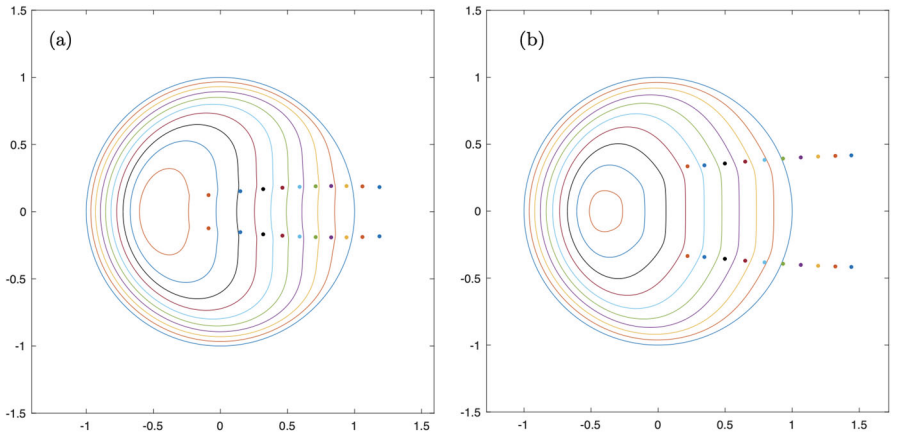


**Fig. 9** The erosion of initially circular bodies with **a** $r_0 = 1.2$, $0 \leq t \leq 0.15$, **b** $r_0 = 1.5$, $0 \leq t \leq 0.175$. Dots show equilibrium vortex locations with the color of each dot corresponding to the same color interface

In a similar procedure to that of Sect. 3.1 Algorithm 1, MATLAB routines *ode15i* and *fminsearch* were used to solve the coupled system of ODEs at each point on the boundary of the half-disk and to find the equilibrium location of the vortices at each timestep from the Hamiltonian (25). In the latter routine, it is required to give an initial guess for the equilibrium location at a particular timestep $t = T$. For this estimate, it proves sufficient to use the equilibrium location implied by the Hamiltonian (24) since this can be computed accurately from (30) and (31) (applied at $t = T$ rather than $t = 0$), by first finding $r_T$ and then $y_T$ and $x_T$. From this estimate, *fminsearch* is able to successfully find the actual equilibrium location in the $z$-plane at $t = T$.

### 4.4 Circular bodies

Figure 9 shows the erosion of two initial circular disks and corresponding vortex positions. Two different initial locations of the Föppl pair are presented: $r_0 = 1.2$ and $r_0 = 1.5$. Not surprisingly erosion proceeds more quickly (i.e., greater change of area with time) in the case that the vortices are initially located closer to the body. In both cases, the erosion proceeds more rapidly at the rear of the body and typically acts to flatten the body at its rear. This has some similarity to the results reported in [1, 2] which also shows a flattening at the rear; however, in their experimental and numerical results, the front of the boy erodes more rapidly than here.

Figure 9 also shows the front of the body maintaining its curvature while it erodes. This is also in contrast to [1, 2] where the erosion produced a sharpening of the leading edge so that the body eroded toward a triangular shape.

Figure 10 shows streamlines and contours of the Hamiltonian for an initially circular disk at $t = 0.25$ for the case when $r_0 = 1.2$. As expected, contours of the Hamiltonian are closed in the lee of the body indicating that the vortex equilibria are stable.

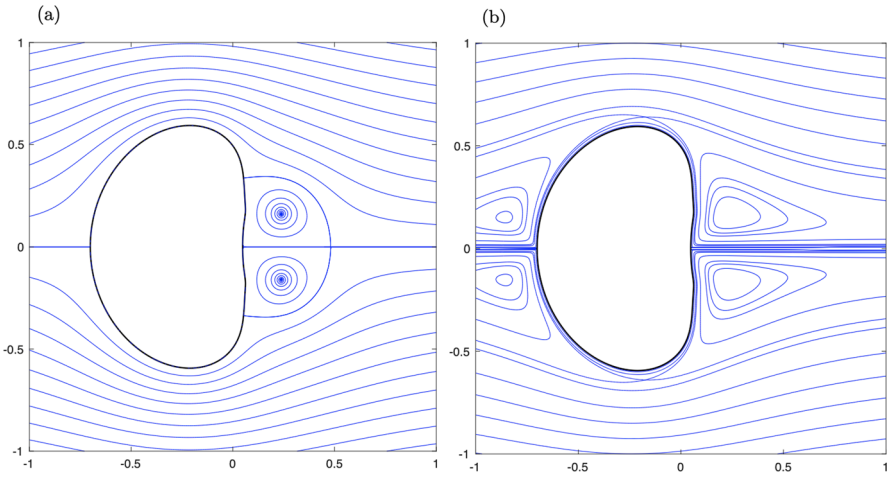


**Fig. 10** Streamlines (**a**) and Hamiltonian contours (**b**) after the initial circle has undergone erosion to $t = 0.25$. The initial vortex locations are $r_0 = 1.2$

### 4.5 Other starting shapes

Other initial starting shapes which are symmetric about the Re$(z)$-axis are readily studied using this method; all that is required is the initial map $z = h(\zeta, 0)$ in its truncated form. Here, examples of bodies with elliptical and triangular-like initial boundaries are presented. In the elliptical case, one symmetry axis is aligned in the flow direction and has length $1 + \lambda$ and the other has length $1 - \lambda$, $-1 \leq \lambda \leq 1$. This geometry implies in (22) the choice $C(0) = 1$, $c_1(0) = \lambda$ and all other $c_n(0) = 0$. To initiate the numerical experiment, Föppl-type equilibrium vortices located behind the ellipse are specified using the formulae of Hill [20] which are presented (and a correction to them given) in Appendix C with the choice $r_s = 1.2$.

Figure 11 shows the evolution of two elliptical bodies with $\lambda = \pm 0.2$. Again, the rear of the body erodes more quickly being closer to the vortices, with the vortices approaching the body as it erodes in order to maintain equilibrium. The typical flattening of the body on the lee side and eventual concave shape that occurs for initially circular bodies is also evident for these elliptical starting shapes.

Figure 12 shows the evolution of two initial triangular shaped bodies generated using the map $z = C(0)\zeta + c_2(0)\zeta^{-2}$ where $C(0) = 1$ and $c_2(0) = \pm 0.29$ with the sign of $c_2$ determining whether the pointy side of the triangle on the Re$(z)$-axis faces upstream or downstream. In this case, the strength of the fixed circulation $\Gamma = \pm 1.19$ is chosen and the equilibrium location of the vortex pair at $t = 0$ found numerically from the Hamiltonian using *fminsearch*. Again the body erodes in a manner akin to both the circular and elliptical cases with a flattening on the lee side, and suggests that arbitrary shaped bodies would erode similarly.

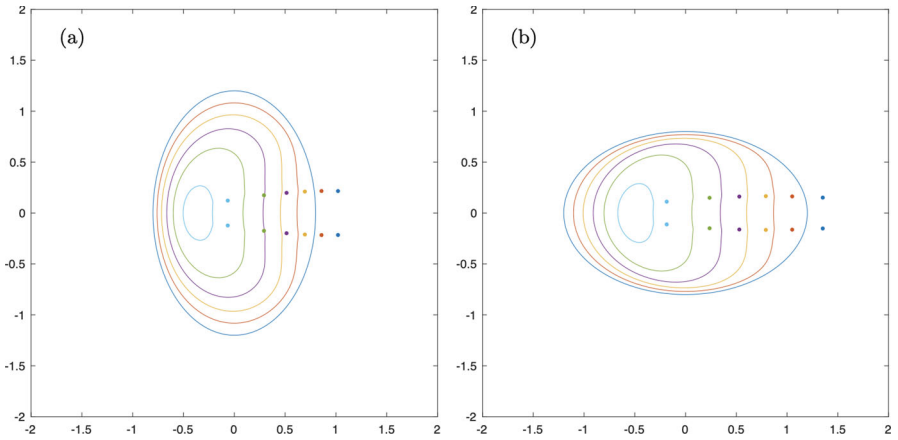


**Fig. 11** The erosion of initially elliptical bodies with **a** $\lambda = -0.2$, $0 \leq t \leq 0.135$ and **b** $\lambda = 0.2$, $0 \leq t \leq 0.1505$. Dots show equilibrium vortex locations with the color of each dot corresponding to the same color interface

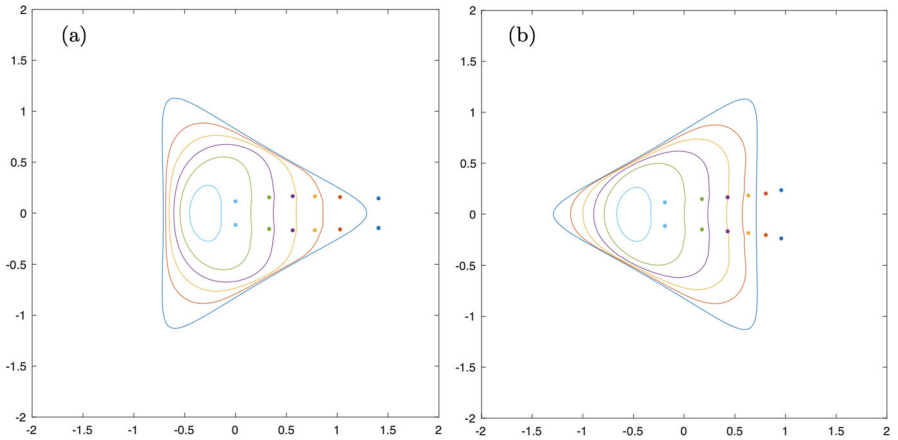


**Fig. 12** The erosion of initially triangular bodies, with $\Gamma = -1.19$. **a** $c_2(0) = 0.29$, $r_0 = 1.4$ and $0 \leq t \leq 0.115$. **b** $c_2(0) = -0.29$, $r_0 = 0.99$ and $0 \leq t \leq 0.12$

## 5 Conclusion

Two problems for the co-evolution of the flow past a slowly eroding fluid–solid interface have been considered. Both problems involve trapped vortices in equilibrium with the surface or solid body and the background flow. The presence of point vortices indirectly models the effect of viscosity since vortex formation is often the result of shedding of viscous boundary layers from a solid surface. Confining the vorticity to singular points together with the assumption of an inviscid fluid allows methods of conformal mapping to be employed on both the free boundary problem and in finding the equilibrium location of the vortices. The downside is that the erosion law is not able to be based directly on the surface shear stress of a viscous boundary layer since

there is none. Instead we use erosion laws which attribute the erosion rate to some function of the tangential velocity at the fluid–solid interface. This ad-hoc assumption seems reasonable on the basis that the ability of fluid to remove and transport particles from a substrate is likely proportional to its local speed and that vortex structures will enhance this ability.

The erosion laws are chosen so that they preserve some sort of symmetry in the eroding surface or solid body. That is, a symmetric valley about the $\mathrm{Im}(z)$-axis in the first problem and a symmetric finite body about the $\mathrm{Re}(z)$-axis in the second. A possible extension to the work is to consider variants of the erosion laws which lead to asymmetric evolution. Mathematically, in such a case, the coefficients in the Laurent series of the conformal map, e.g., (4), need both time-varying real and imaginary parts so effectively doubling the number of unknowns that need to be solved for. Asymmetric evolution of an infinite surface would also allow for accumulation (deposition) of eroded material on the surface. Such a scenario may occur in the erosion of a sandy bed by vortices in the lee of subsea pipelines in which sand is eroded immediately below the vortex and deposited further downstream. Deposition could be incorporated in the numerical approach by changing the sign of the forcing term in the PG equation, though it may be this is an unstable process by analogy with e.g., ice accumulation [23] and Hele–Shaw flow [25].

In both problems, as the erosion continues the vortices move toward the eroding interface in order to maintain equilibrium. In the infinite surface problem, the valley continues to be eroded downward for all time. In the second problem, the body is completely eroded in finite time. Results showing the flattening of the rear of the finite body irrespective of the starting shape are reminiscent to the experiments of [1, 2] and suggest that inclusion of shed vorticity in the form of trapped vortices in the wake is a significant contributor to the erosion of finite bodies in uniform flow.

Numerical conformal mapping techniques such as those based on AAA-least squares [30] or SC Toolbox [31] coupled with the PG formulation of the present work would enable the consideration of more exotic starting shapes than those presented here e.g., asymmetric polygons.

## Appendix A: Exact solution for a fixed vortex

When the vortex remains fixed at $z = \mathrm{i}$ and the initially flat surface coinciding with $\mathrm{Re}(z)$ erodes due to the erosion law given in model I, an analytical solution can be found. This is somewhat artificial in that it does not respect the non-zero velocity at the vortex which would in general cause it to drift but it is a useful solution for checking numerical results. In this case, $\zeta_0 = 0$ for all time and the PG equation (18) becomes

$$\mathrm{Re}\left[\overline{f'\zeta}\,\dot{f}\right] = \alpha, \tag{A1}$$

where $\alpha = \beta|\Gamma|/2\pi > 0$ is a constant. Given the constant term on the right hand side, (A1) is analogous to the Hele–Shaw free boundary flow for a source of unit strength [24, 25].

Following [26, 27] let

$$z = \frac{\mathrm{i}A}{\zeta + 1} + \mathrm{i}a_0 + \mathrm{i}a_1\zeta. \tag{A2}$$

This is a truncated form of (4) and turns out to be sufficient to obtain an exact solution of (A1). Note (A2) can be expressed as

$$z = \frac{2\mathrm{i}(1 - a_1)}{\zeta + 1} + \mathrm{i}(2a_1 - 1) + \mathrm{i}a_1\zeta, \tag{A3}$$

where we have used (5) and the truncated version of (7) up to and including the $a_1$ term. By direct substitution of (A3) into (A1) and simplifying gives precisely $\dot{a}_1(3a_1 - 1) = \alpha$. Using $a_1(0) = 0$, this then gives

$$a_1 = \frac{1 - \sqrt{1 + 6\alpha t}}{3}, \tag{A4}$$

so that (A3) and (A4) give the exact solution of the evolving interface in parametric form where $\zeta = \exp(\mathrm{i}\theta)$, $-\pi < \theta < \pi$.

Alternatively, in close analogy to [26, 27], the exact solution can be obtained by considering the Schwarz function of the curve representing the interface. The Schwarz function, denoted by $S(z, t)$, is a function which is analytic in the neighborhood of the curve $\partial\Omega$ and such that $S(z, t) = \overline{z}$ on $\partial\Omega$. Two properties of the Schwarz function useful here are [32]

$$\frac{\mathrm{d}z}{\mathrm{d}s} = \frac{1}{\sqrt{S'}}, \tag{A5}$$

and

$$\upsilon_n = -\frac{\mathrm{i}\dot{S}}{2\sqrt{S'}}, \tag{A6}$$

where again, $\upsilon_n$ represents the normal velocity to $\partial\Omega$, $s$ is an along-$\partial\Omega$ coordinate and $S' = \partial S/\partial z$. Since the interface is a streamline, we can write (10) as

$$\upsilon_n = \beta\frac{\partial\phi_V}{\partial s}\bigg|_{\partial\Omega} = \beta\frac{\partial F_V}{\partial z}\frac{\partial z}{\partial s}\bigg|_{\partial\Omega}, \tag{A7}$$

where the subscript $V$ indicates the erosion model I assumption, namely it is only the flow due to the vortex that causes erosion.

Using (A5) and equating (A6) and (A7), we obtain

$$\dot{S} = 2\mathrm{i}\beta\,\mathrm{sgn}(\Gamma)\frac{\partial F_V}{\partial z}\bigg|_{\partial\Omega}, \tag{A8}$$

where the factor sgn($\Gamma$) is required so as to produce erosion (rather than growth) of the surface.

Using the map (A3) and taking its conjugate, with $\overline{\zeta} = \zeta^{-1}$ on $\partial\Omega$, gives the Schwarz function of $\partial\Omega$

$$S = z - \mathrm{i}a_1(\zeta + \zeta^{-1}) - 2\mathrm{i}a_1, \tag{A9}$$

showing that $S$ is singular at $\zeta = 0$, the pre-image of the vortex location $z = \mathrm{i}$. As $z \to \mathrm{i}$, we know $F_V \to -(\mathrm{i}\Gamma/2\pi)\log(z - \mathrm{i})$ and hence $\partial F_V/\partial z$ is singular as $z \to \mathrm{i}$. By analytic continuation, (A8) holds as $z \to \mathrm{i}$, and so $\dot{S}$ must also be singular in this limit such that (A8) is satisfied. Now, from (A3) we have

$$z - \mathrm{i} \sim \mathrm{i}\zeta\,(3a_1 - 2) \quad \text{as} \quad z \to \mathrm{i}, \zeta \to 0, \tag{A10}$$

and so (A8) gives

$$\frac{\mathrm{d}}{\mathrm{d}t}\left(3a_1^2 - 2a_1\right) = \frac{\beta\,|\Gamma|}{\pi} = 2\alpha, \tag{A11}$$

which when solved subject to $a_1(0) = 0$ gives (A4).

## Appendix B: The eroded area in terms of conformal map coefficients

Using the complex form of Green's theorem, the area $\Delta$ for any closed contour in the $z$-plane is given by

$$\Delta = \frac{1}{2\mathrm{i}}\oint_{\partial\Omega}\overline{z}\mathrm{d}z = \frac{1}{2\mathrm{i}}\oint_{|\zeta|=1}\overline{z}\frac{\mathrm{d}z}{\mathrm{d}\zeta}\mathrm{d}\zeta, \tag{B12}$$

where $z(\zeta)$ is a conformal map from the unit $\zeta$-disk to the interior of the closed contour in the $z$-plane. In the first problem, the contour representing the interface closes at infinity and the area of the region above the contour is unbounded. Calculation of the area can be renormalized by subtracting off the area of the upper half plane above the Re($z$)-axis to obtain the finite area $\Delta$ between the interface and the Re($z$)-axis.

Using the symmetric version of (4) and the map from the unit $\zeta$-disk to the upper half $z$-plane given by $z_f = \mathrm{i}A/(\zeta+1) - \mathrm{i}A/2$, which has the same asymptotic behavior as the map (4) as $z \to \infty$, we obtain

$$\begin{aligned}\Delta = \frac{1}{2\mathrm{i}}\oint_{|\zeta|=1}&\left(-\frac{\mathrm{i}A\zeta}{\zeta+1} - \mathrm{i}a_0 - \mathrm{i}\sum_{n=1}^{\infty}\frac{a_n}{\zeta^n}\right)\left(-\frac{\mathrm{i}A}{(\zeta+1)^2} + \mathrm{i}\sum_{n=1}^{\infty}n a_n\zeta^{n-1}\right)\\ &-\left(-\frac{\mathrm{i}A\zeta}{\zeta+1} + \frac{\mathrm{i}A}{2}\right)\left(-\frac{\mathrm{i}A}{(\zeta+1)^2}\right)\mathrm{d}\zeta,\end{aligned} \tag{B13}$$

where the last term inside the integral represents the contribution from $\overline{z_f}\mathrm{d}z_f/\mathrm{d}\zeta$.

Expanding the products and neglecting terms with no simple poles (and so do not contribute to the contour integral), (B13) is equivalent to

$$\Delta = \frac{1}{2\mathrm{i}} \oint_{|\zeta|=1} \left( \frac{A\zeta}{\zeta+1} \sum_{n=1}^{\infty} n a_n \zeta^{n-1} - \frac{A}{(\zeta+1)^2} \sum_{n=1}^{\infty} \frac{a_n}{\zeta^n} + \sum_{m=1}^{\infty} \sum_{n=1}^{\infty} \frac{a_m}{\zeta^m} n a_n \zeta^{n-1} \right) d\zeta, \tag{B14}$$

which can be simplified further to

$$\Delta = \frac{1}{2\mathrm{i}} \oint_{|\zeta|=1} \frac{1}{\zeta} \left( \sum_{n=1}^{\infty} n a_n^2 + A \sum_{n=1}^{\infty} n(-1)^n a_n \right) \mathrm{d}\zeta, \tag{B15}$$

upon retaining only terms in the integrand corresponding to order one poles. Applying the residue theorem to (B15) gives

$$\Delta = \pi \sum_{n=1}^{\infty} \left( n a_n^2 + n(-1)^n A a_n \right). \tag{B16}$$

## Appendix C: Föppl equilibria for an ellipse

Here, we give the formula derived by [20] for equilibrium vortices trailing an ellipse immersed in a uniform flow with unit speed at infinity in the direction of increasing $\mathrm{Re}(z)$, and with a symmetry axis of the ellipse aligned with the $\mathrm{Re}(z)$-axis. Hill [20] uses $z = \zeta + \lambda a^2/\zeta, -1 < \lambda < 1$, to map from the exterior of the ellipse to the exterior of a circle of radius $a$ in the $\zeta$-plane. Now put $a = 1$, and let $\zeta_0 = r_s \exp(\pm \mathrm{i}\theta_s)$ be the pre-image location of the equilibrium vortices. Then [20]

$$\sin^2 \theta_s = \frac{(r_s^2 - 1)^2 (r_s^2 - \lambda)}{4(r_s^6 - \lambda)}, \tag{C17}$$

and

$$\Gamma = -2\pi \frac{(r_s^2 - 1)^2 (1 + r_s^2)(r_s^4 - \lambda)^2}{r_s (\lambda^2 + \lambda r_s^8 - 2\lambda r_s^6 - 2\lambda r_s^4 + \lambda r_s^2 + r_s^{10})} \sqrt{\frac{r_s^2 - \lambda}{r_s^6 - \lambda}}, \tag{C18}$$

where $\Gamma < 0$ is the circulation of the vortex in the upper half of the $\zeta$-plane. Note that (C17) is the same as in [20] but (C18) provides a correction to eq. (1.32) of [20] (and also eq. (49) of [33]): specifically $\lambda^2$ replaces $\lambda$ in the first term inside $(\cdots)$ in the denominator of (C18). This correction was subsequently verified in two ways: (i) repeating the derivation of [20] employing Wolfram *Mathematica* to perform some of the algebra; (ii) comparing the location of the equilibria for given $\lambda \neq 0$ and $r_s$ using (C17) and that found by constructing the Hamiltonian for the ellipse for vortices with

circulation given by (C18) and finding the equilibria numerically using MATLAB's *fminsearch* applied to the Hamiltonian.

**Acknowledgements** We thank the reviewers for their helpful comments.

**Author contributions** C.H. and N.R.M. contributed equally to the writing of the manuscript and in formulating the problems, and their investigation by analytical and numerical techniques.

**Funding** Courteney Hirst was supported by a UK Engineering and Physical Sciences Research Council PhD studentship, grant numbers EP/T517793/1 and EP/W524335/1.

**Data availability** No datasets were generated or analyzed during the current study.

## Declarations

**Competing interests** The authors declare no competing interests.



## References

1. Ristroph L, Moore MNJ, Childress S, Shelley MJ, Zhang J (2012) Sculpting of an erodible body by flowing water. Proc Natl Acad Sci 109(48):19606–19609
2. Moore MNJ, Ristroph L, Childress S, Shelley MJ, Zhang J (2013) Self-similar evolution of a body eroding in a fluid flow. Phys Fluids 25(11):116602
3. Ristroph L (2018) Sculpting with flow. J Fluid Mech 838:1–4
4. Devauchelle O, Petroff AP, Seybold HF, Rothman DH (2012) Ramification of stream networks. Proc Natl Acad Sci 109(51):20832–20836
5. Meakin P, Jamtveit B (2010) Geological pattern formation by growth and dissolution in aqueous systems. Proc. R. Soc. A 466(2115):659–694
6. Curl RL (1966) Scallops and flutes. Trans. Cave Res. Group Great Britain 7:121–160
7. Bushuk M, Holland DM, Stanton TP, Stern A, Gray C (2019) Ice scallops: a laboratory investigation of the ice-water interface. J Fluid Mech 873:942–976
8. Douglas TA, Mellon MT (2019) Sublimation of terrestrial permafrost and the implications for ice-loss processes on Mars. Nat. Commun. 10(1):1716
9. Laity JE, Bridges NT (2009) Ventifacts on earth and mars: analytical, field, and laboratory studies supporting sand abrasion and windward feature development. Geomorphology 105:202–217
10. Goldenfeld N, Chan PY, Veysey J (2006) Dynamics of precipitation pattern formation at geothermal hot springs. Phys Rev Lett 96:254501
11. Grodzki P, Szymczak P (2019) Reactive-infiltration instability in radial geometry: from dissolution fingers to star patterns. Phys Rev E 100:033108
12. Huang JM, Moore NJ (2022) Morphological attractors in natural convective dissolution. Phys Rev Lett 128:024501
13. Thomas RM (1979) Size of scallops and ripples formed by flowing water. Nature 277(5694):281–283
14. Whitney MI (1979) Electron micrography of mineral surfaces subject to wind-blast erosion. GSA Bull 90(10):917–934

15. Lee JY, Forrest AL, Hardjanto FA, Chai S, Cossu R, Leong ZQ (2018) Development of current-induced scour beneath elevated subsea pipelines. J Ocean Eng Sci 3(4):265–281
16. Song S, Park S (2022) Unresolved CFD and DEM coupled simulations on scour around a subsea pipeline. J Mar Sci Eng 10(5):556
17. Semenov YA, Wu GX (2016) Cratering of a solid body due to liquid impact. J Eng Math 101(1):71–85
18. Lamb H (1932) Hydrodynamics. Cambridge University Press, Cambridge
19. Saffman PG (1993) Vortex dynamics. Cambridge University Press, Cambridge
20. Hill DJ (1998) Part I. Vortex dynamics in wake models. Part II. Wave generation. PhD thesis, California Institute of Technology
21. Zannetti L (2006) Vortex equilibrium in flows past bluff bodies. J Fluid Mech 562:151–171
22. Vasconcelos GL, Moura MN, Schakel AMJ (2011) Vortex motion around a circular cylinder. Phys Fluids 23(12):123601
23. Cummings LM, Hohlov YE, Howison SD, Kornev K (1999) Two-dimensional solidification and melting in potential flows. J Fluid Mech 378:1–18
24. Gustafsson B, Vasiliev A (2009) Conformal and potential analysis in Hele-Shaw cells. Birkhauser, Basel
25. Howison SD (1986) Fingering in Hele-Shaw cells. J Fluid Mech 167:439–453
26. McDonald NR (2010) Computation of Hele-Shaw free boundary problems near obstacles. Theoret Comput Fluid Dyn 24(6):537–550
27. Jiang Y, McDonald NR (2022) Dissolution of plane surfaces by sources in potential flow. Phys D 442:133549
28. Dallaston MC, McCue SW (2013) An accurate numerical scheme for the contraction of a bubble in a Hele-Shaw cell. In: Proceedings of the 16th Biennial computational techniques and applications conference, CTAC-2012. ANZIAM J., vol 54, pp 309–326
29. Crowdy DG (2023) Exact solutions for steadily travelling water waves with submerged point vortices. J Fluid Mech 954:47
30. Trefethen LN (2020) Numerical conformal mapping with rational functions. Comput Methods Funct Theory 20(3):369–387
31. Driscoll TA (1996) Algorithm 756: a MATLAB toolbox for Schwarz-Christoffel mapping. ACM Trans Math Softw 22(2):168–186
32. Davis PJ (1974) The Schwarz function and its applications. Math. Assoc. America, Washington
33. Kanso E, Oskouei BG (2008) Stability of a coupled body-vortex system. J Fluid Mech 600:77–94